Assembly of mobile 5G transceiver based on photonic motherboard

Bradley W. Snyder[a], Zerihun G. Tegegne[a], Nienke Nijenhuis[a], Tianwen Qian[b], David de Felipe[b], Simon Nellen[b], Milan Deumer[b], Y. Durvasa Gupta[b], Moritz Baier[b], Björn Globisch[b], Norbert Keil[b], and Joost Van Kerkhof[a]

[a]PHIX Photonics Assembly, De Veldmaat 17, 7522 NM Enschede, Netherlands
[b]Fraunhofer Heinrich Hertz Institute, Einsteinufer 37, 10587 Berlin, Germany

ABSTRACT

We describe the assembly of a 5G transceiver leveraging photonics for the generation, emission and detection of THz wireless signals. The transceiver and all associated control electronics and power supplies are designed for mounting in a mobile aerial unit. A photonics motherboard concept that brings together polymer, III-V and SiN-based photonic platforms and provides optical fiber connectivity is used for the assembly. In addition, scalable integration of 3D components, in this case an antenna rod or rod array, is demonstrated. Thermal considerations arising from the dense integration of photonic and electronic components and the resulting concentrated heat load are also discussed.

Keywords: Photonics, hybrid integration, 5G, transceiver, photonic motherboard

1. INTRODUCTION

The demand for increased bandwidth continues to grow with both the population and the sophistication of computer and smartphone applications. To try to meet this demand, incremental improvements in wireless technology are realized by the engineers of the world. Current and upcoming standards such as 5G and 6G ensure that devices from multiple vendors can work together.[1]

Wireless channel bandwidth is fundamentally limited by the carrier frequency. Traditional radio frequency channels with carriers up to the SHF range (super high frequency = 3 GHz to 30 GHz, wavelength = 10 cm to 1 cm) are limited to a few MHz each. By moving to the millimeter-wave region, the carrier frequency is increased by an order of magnitude to 30 GHz to 300 GHz, bringing an increase in channel bandwidth along with it, but with additional complexity. This trend continues also into the terahertz region of 0.3 THz to 3 THz. In particular, signals in the millimeter-wave region and beyond experience more attenuation in free-space propagation than those at lower frequencies. This means that wireless access points need to be placed closer to devices and overall cell sizes are decreased. One way to address this is to have mobile access points. A series of these mobile access points can be deployed to form a mesh that can relay data to fixed backhaul points.

Building this kind of mobile access point is one of the goals of the EU Horizon 2020 TERAWAY project.[2] The project brings together a wide variety of partners across industry and academia in Europe to realize the hardware and software necessary for telecommunications in the W-band (92 GHz–114.5 GHz), D-band (130 GHz–174.7 GHz) and THz band (252 GHz–322 GHz). In particular, the hardware working group is focusing on using integrated optics and hybrid integration of different photonic platforms to design and fabricate a wireless transceiver that can be mounted in a heavy-duty drone. A group of these drones can then be rapidly deployed to provide high-bandwidth data communications in a wide variety of situations, such as music festivals or even crisis management during natural disasters. The following sections of this manuscript will describe in detail some of the challenges of the optical, wireless and thermal integration of such a transceiver, with concrete examples being given from an initial prototype with limited functionality.

Further author information: (Send correspondence to Bradley W. Snyder)
Bradley W. Snyder: E-mail: b.snyder@phix.com
David de Felipe: E-mail: david.felipe@hhi.fraunhofer.de

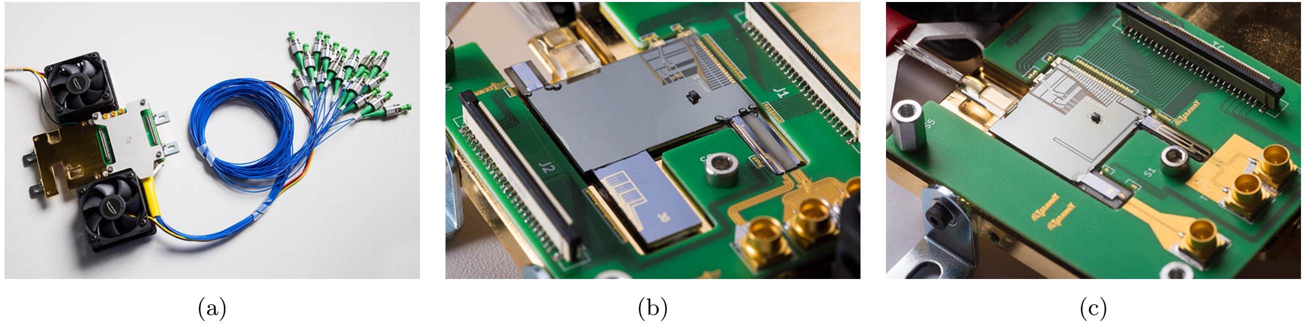

(a) (b) (c)

Figure 1: Completed TERAWAY transceiver modules: (a) transmitter, (b) detail of transmitter, (c) detail of receiver

2. OVERVIEW OF 5G TRANSCEIVER

In order to facilitate a two-way high-speed link, any transceiver must consist of both a transmitter (Fig. 1b) and receiver (Fig. 1c). These two modules are themselves made up of a set of constituent parts implemented in different fabrication platforms.

The transmitter consists of an optical carrier generation unit (including tunable laser source), optical phase locking unit (implemented using an optical frequency comb generator [OFCG]), optical modulation unit, optical filtering unit, optical multi-beamforming unit, and finally an optical amplification, frequency upconversion and wireless emission unit. For these functional units, the majority of the active functions are implemented in Fraunhofer HHI's InP platform, with the exception of a set of tunable Mach-Zehnder Interferometers (MZIs) implemented in the SiN-based TriPleX platform, while the passive functions (splitters, fixed multi-mode interferometer couplers [MMIs]) are spread out across the TriPleX platform and Fraunhofer HHI's polymer waveguide-based PolyBoard platform. In addition to the integrated photonics platforms, a fiber interface is also provided to enable the assembly process as well as to provide visibility into the system for initial tests.

The receiver shares the optical carrier generation unit and OFCG of the transmitter and introduces an optical phase shift unit, and a wireless detection and IQ photonic mixing unit for coherent detection. The receiver implements all of this functionality in the InP and PolyBoard platforms, with the latter platform containing the passives and tunable phase shifters with the rest of the functions in the former. Further details on the design and function of these units can be found in.[3–9]

In both the transmitter and receiver, the concept of a photonic motherboard is employed. By this it is meant that a single large chip serves as the attach point and routing platform for several smaller chips. In this case, the PolyBoard serves as the motherboard, and the InP and SiN chips, as well as the fiber array, are all attached at the various edges of the PolyBoard.

Integrating all of these components across multiple platforms requires a complicated multi-step process. Technical considerations, such as which components and adhesives can withstand certain temperatures, or how components can be handled with fragile and protruding parts such as an 8 mm long silicon antenna rod, must be balanced out with more practical considerations, such as the capabilities present in the various project partner facilities, and avoiding too many journeys in the post. In the end, the project partners agreed on a process flow for the assembly of both the transmitter and receiver modules that includes the following steps:

1. Active components are attached to PolyBoard at Fraunhofer HHI
2. PolyBoard is shipped to PHIX Photonics Assembly
3. Antenna rod is attached to antenna die
4. Fiber array is attached to PolyBoard
5. TriPleX chip is attached to PolyBoard (transmitter only)

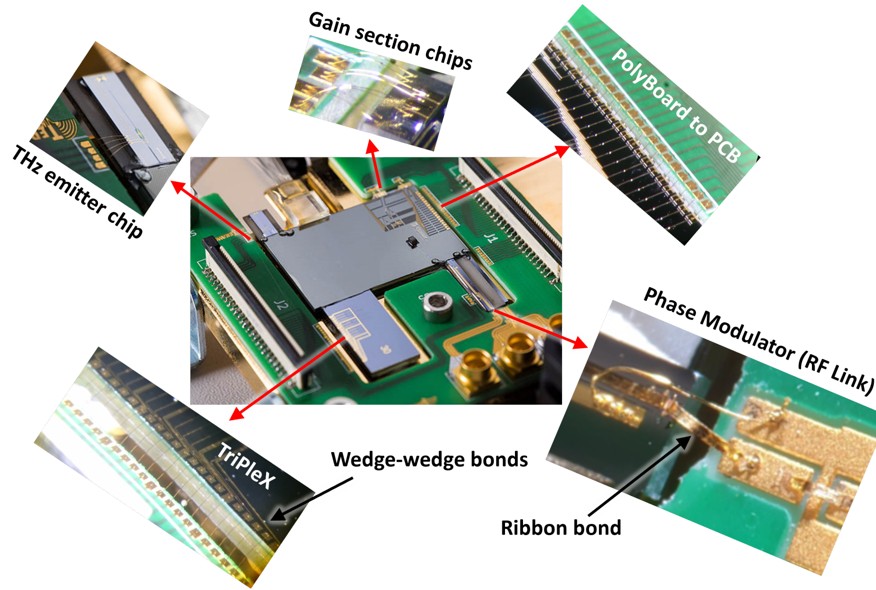

Figure 2: Wire bonding of various components to PCB including DC wedge bonding and RF ribbon bonding

6. Optical subassembly and PCB are mounted to copper submount
7. Wire bonding is performed to electrically connect the various components (Fig. 2)
8. Mechanical build-up of copper submount and thermal subassembly is performed (Peltier thermoelectric cooler, heat bus, heat sinks and fans)

Of these steps, this paper will describe the mechanics of 1 and 3-5 in detail, as well as the design considerations and trade-offs of 8, in the following sections.

3. HYBRID INTEGRATION OF PHOTONIC COMPONENTS

The optical interfacing of the components to the photonic motherboard is performed by active alignment, and they are then affixed with UV-cure epoxy. Where possible, alignment loops are used to simplify the alignment approach. For some active devices, electrical driving is required to realize alignment. The various procedures employed are detailed in the following sections.

3.1 Active components

The attach of the compound semiconductor components, such as the tunable lasers, phase modulators and antenna chips, was performed at the facilities of Fraunhofer HHI. An active alignment process was employed, whereby the components were electrically probed during alignment (Fig. 3a). Furthermore, a fiber was temporarily aligned to one of the ports of the PolyBoard to either inject light or monitor output light.

The small dies were mounted on ceramic submounts to provide extra support while they were clamped in six degree-of-freedom motion stages. Once alignment was optimized, UV cure adhesive was dispensed. This adhesive was dispensed such that a fillet was formed on either side of each die to provide additional bonding strength. This was necessary because the available area for UV illumination was limited by the fact that the substrate of the PolyBoard, as well as the compound semiconductor chips and their ceramic submounts, are opaque with respect to UV illumination. The results in a so-called “shadow cure.”

While this process is currently done manually at Fraunhofer HHI, it is also a process that is available in a fully-automated capacity at PHIX. For the first several builds, it was considered advantageous to perform this process at the home of the dies so that any initial problems could be troubleshooted. PHIX performs such an

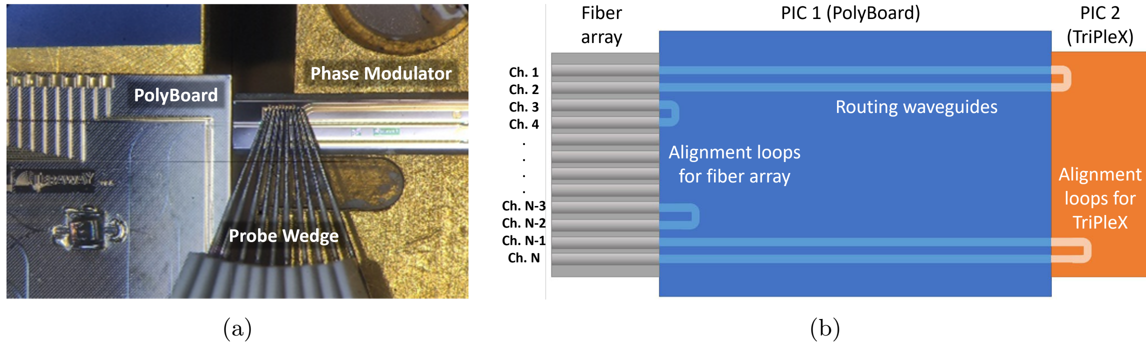

(a) (b)

Figure 3: Alignment strategies used for optical integration: (a) active alignment using electrical probing and (b) loopback waveguides for fiber array and chip-to-chip attach

integration of III-V gain sections to SiN TriPleX chips for commercial products using a fully-automated ficonTEC system. This system has probe pins integrated into the die pickup tool such that the die can be clamped, probed and manipulated all in a single step.

3.2 Fiber attach

After attach of the active components, the subassembly was shipped to the facilities of PHIX. The first step at PHIX was the attach of the antenna rod, which is detailed later in this document. After this, the fiber array was attached. This was done with an active alignment process relying on loopback waveguides (Fig. 3b), which is consistent with the published packaging design rules of PHIX.[10] These loopbacks consisted of four optical ports, two each at the extreme ends of the fiber array. The two ports on each side were connected with a loop waveguide, such that light injected into one port could be measured out the other port. The alignment of the fiber array to the subassembly is then performed using a single set of motion stages with three linear and three rotational degrees of freedom.

This strategy of multiple loops is advisable for first prototypes and provides a few key advantages. First of all, the roll alignment of the fiber array can be directly measured and corrected for. By using a motorized motion stage to move the fiber array perpendicular to the loops, the position of the loops can be determined by the position of maximum coupling. When the maximum coupling occurs at the same scan position, the roll alignment is considered to be optimized. In practice, this results in position errors of less than 50 nm, at which point the core position errors of the fibers themselves will dominate.

Another advantage of the two-loop strategy is the ability to get a first-order measure of the waveguide loss and a more accurate determination of the actual coupling loss independent of the waveguide loss. By making the two loops of significantly different length, a fit can be made considering the measured insertion losses of the loops and the lengths of the loops. This serves as a sort of "packaging PCM" (Process Control Monitor). The main caveat of this is that with only two points for a fit there is room for significant error, especially with low-loss waveguides, due to variation from, e.g., mating losses of connectors during the measurement, fiber core position variation, etc. When there are extra fiber ports available on a device, the accuracy of this PCM can be improved by including a third loop of yet another length to provide a third fitting point.

A UV-cure adhesive was also used to attach the fiber array. Because the fiber array itself is transparent to UV, illumination could be directed through the array itself at the bond line and there was no concern of shadow curing.

3.3 Passives and filters

Similarly as in the case of the fiber attach, the integration of the TriPleX chip relied on loopback waveguides. However, the access to the waveguides in the TriPleX used the already-attached fiber array for injecting and measuring light. This avoids the case where two components, the fiber array and the TriPleX, would need to be manipulated and aligned at the same time. Such a scheme would require two sets of six-axis stages working in parallel, whereas this method requires only one. Furthermore, the finding of "first light" is also greatly simplified

in that only one interface needs to be roughly aligned rather than two interfaces in parallel. This allows for a blind search at one interface without assuming that the other interface is already close enough to being aligned to be able to measure coupled light.

To implement this, four additional channels of the fiber array are coupled to four additional ports in the PolyBoard, which are then routed to the other side of the PolyBoard chip where they are coupled to two loops in the TriPleX chip (Fig. 3b). During the alignment process, the PolyBoard is used as a clamping point for the already-integrated portion of the optical assembly, and the TriPleX is clamped on its own.

Once alignment has been achieved, a small gap is opened between the PolyBoard and the TriPleX chip, and UV cure epoxy is dispensed in a capillary process. As compared to the case of attaching the fiber array to the PolyBoard, a more liberal application of epoxy is performed in order to create a larger amount of fillet at the two sides of the bond. This is to mitigate the fact that both the PolyBoard and TriPleX chips have silicon substrates that are opaque to the wavelength of the UV cure irradiation, resulting in shadowed areas. A cationic epoxy was used, which partially mitigates this issue by having a cure that propagates approximately 100 µm into these shadow regions. Furthermore, a thorough post-bake aids in completing the cross-linking of the epoxy.

3.4 Scaling to higher volume

In the last two assembly steps, a total of 8 channels in a fiber array are required to enable the active alignment processes. This might at first seem onerous, especially when considering the non-linear cost scaling of the polarization-maintaining fibers (PMF) used for these modules. However, having permanent attach to these loops is very helpful in the initial stages of prototyping a product. Being able to monitor the coupling losses through the loops during the various subsequent assembly—additional optical attaches, wire bonding and mechanical build-up—gives insight into the stability of the assembly and enables troubleshooting.

For scaling to higher volumes, an approach without permanent attach of the fibers can be used. In this case, the loops are still included on the integrated photonic components, as they essentially come for free, and the fiber array is used as a probe during the assembly of other components. This means that the fiber array itself needs to be mounted on its own set of six-axis stages and needs to be realigned for every optical attach. Still, the use of loopback structures makes this alignment quick and relatively straightforward, especially when compared to other processes where two fibers or fiber arrays need to be aligned in parallel to opposite sides of a chip.

4. ANTENNA ROD ASSEMBLY

One of the key challenges in realizing the transceiver assemblies is the integration of an approximately 8 mm long silicon antenna rod that protrudes out from the substrate of the InP antenna die. For the antenna rod to function efficiently, it needs to be within 100 µm of the center of the bow-tie antenna, and it needs to be perpendicular to this antenna. Further complicating this is the fact that the only alignment references are on the device (top) side of the InP die, while the rod is attached to the substrate (bottom) side of the die. Once the rod is attached, there is also an obvious challenge from the standpoint of handling, as the lower surface of the optical assembly is no longer planar.

To tackle the more straightforward issue of handling the subassembly during antenna rod attach and thereafter, a standard PHIX chip clamp was modified to have deeper clamping fingers (at the right in Fig. 5c). This allowed the subassembly to be mounted in the clamp, and then both pieces could be flipped over during the rod attach. The clamp normally has enough base height such that when it is flipped right-side up, the antenna rod will have still have plenty of clearance to other tooling.

4.1 Molded vacuum tool fabrication

The more interesting challenge was to create tooling to hold the antenna rod (and later array). The rod itself has a square base, but tapers to a thin, sharp edge along one dimension. In the other dimension, it stays at a constant thickness of only 350 µm (Fig. 4). After some discussion with the team at Finetech, the producer of the FINEPLACER® Lambda flip-chip tool used for the first assemblies, it was decided to use a molding process to make a vacuum holder. This concept, when combined with a generic vacuum tool, would allow us to fabricate

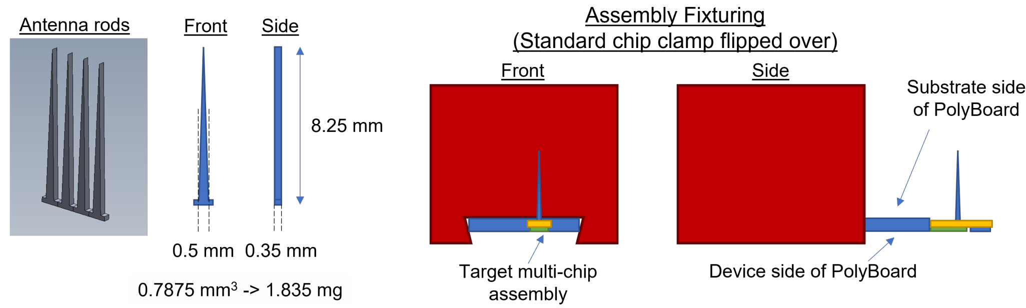

Figure 4: Schematic of antenna rod (single and 1 × 4 array) and assembly fixturing

fixturing for any number of structures, whether it is the single antenna rod in this iteration of the 5G transceiver, or the 4 × 4 antenna rod arrays to be used in later iterations with beam steering.

Before a mold could be made, first there needed to be something to mold. Therefore, a so-called "golden sample" was made (Fig. 5a). This consisted of an antenna rod glued to a glass slide with a small glass standoff. Because the fabrication of this part only needed to be done once, a more *ad hoc* solution could be employed. A sample antenna rod was temporarily mounted to a six-axis setup. Prisms and a binocular microscope were used to ensure that the square base was fully parallel to the glass standoff. The reflection of the rod base in the glass aided in this process. The rod was eventually attached using a quick-curing cyanoacrylate adhesive. Finally, it was carefully removed from the mount.

The golden sample was then sprayed with a release agent coating (Polytek Pol-Ease® 2300) and placed upside-down in a cup filled with a molding compound. A two-part compound with no special cure steps was used (Polytek EasyFlo 60). However, the ratio of the two parts was found to be a very sensitive parameter, and thus careful measuring and mixing were required. Furthermore, the reaction of the two components was exothermic, and so care needed to be taken with respect to the choice of vessel for the reaction. Along with the released heat, the compound initially expands and then later contracts as it approaches full cure. These two effects meant that the use of a glass vessel would result in shattering. Instead, plastic was used. On the other hand, the contraction was helpful in that it meant the mold would not be too tight around the antenna rod.

Once the mold had set, the golden sample was removed and the mold was released from the plastic cup. A drill was used to open a hole from the back of the mold to where the point of the antenna rod would later be present. This hole needed to be drilled as parallel to the axis of the antenna rod as possible. The surface where the golden sample had been dipped was used as a reference, and therefore it needed to be kept as flat as possible. After drilling, excess material was trimmed away, and a mark was made to indicate the orientation of the tapered dimension of the rod.

4.2 Modified flip-chip process

For the actual rod attachment process, an antenna rod was manually loaded into the molded piece. This was then mounted to the vacuum tool head of the Lambda flip-chip machine. The position of the antenna chip bow-tie was measured relative to features that could be viewed from the substrate side , such as the antenna die edge or the edges of the AlN submount on which it sat (Fig. 5b). These measurements were then applied, with mirroring where appropriate, when the subassembly was flipped over. Some error could occur due to features lying in different focal planes as well as any tapering of the sidewalls of, in particular, the AlN submount, but these errors were well below the required accuracy of 100 µm. Furthermore, due to imperfections in the back-drilling, some slight shimming had to be applied to ensure the antenna rod ended up completely perpendicular.

When all adjustments had been completed, UV cure adhesive was applied. The damming of this adhesive was aided by the walls of the AlN submount, which has a laser-drilled aperture in the area where the antenna rod would be attached. The rod was then brought down into place and the adhesive was cured. Finally, the vacuum was released and the optical subassembly was lowered straight down using the flip-chip machine's sample stage. This is in contrast to the normal operation where the flip-chip arm is raised. This choice was made due

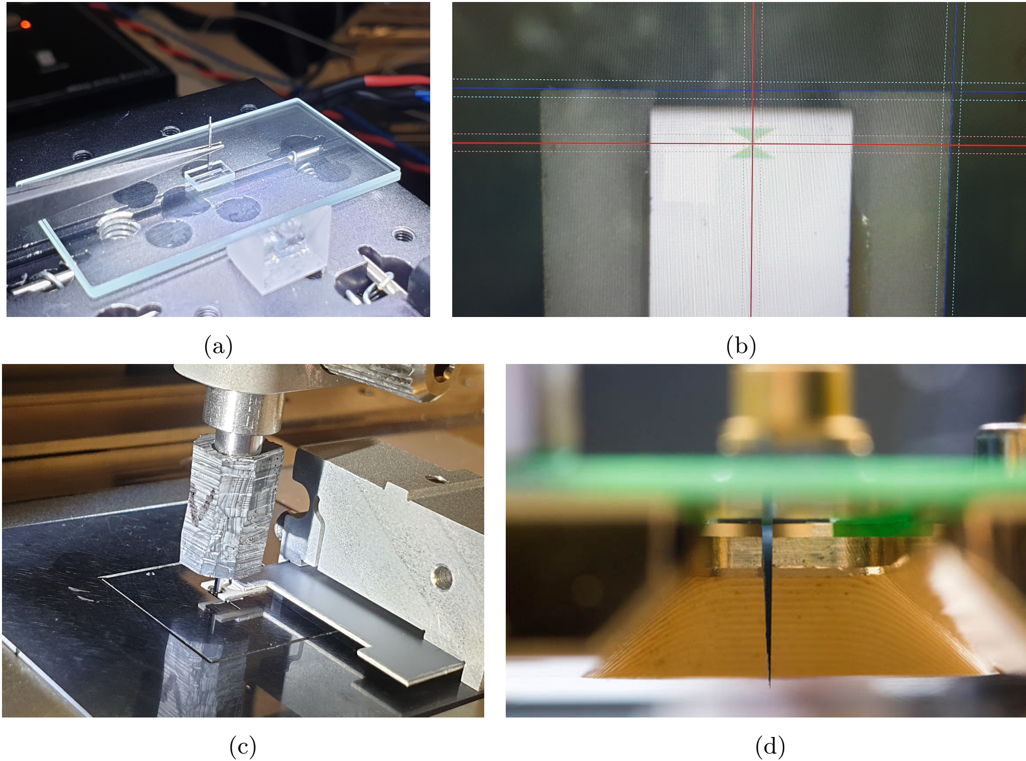

Figure 5: Antenna rod attachment process: (a) fabrication of golden sample for molding, (b) measurements taken from the device side of the antenna die to enable alignment, (c) placement of antenna rod onto substrate side of antenna die, and (d) antenna rod on completed module

to the fact that the flip-chip arm travels in an arc motion, rather than a straight motion, and this would result in damage to the antenna rod. In the end, the process was completed successfully and repeatably on both the transmitter and receiver modules (Fig. 5d).

5. THERMAL DESIGN

The goal of the design of the thermal management system for the transceiver modules is to ensure that the components operate at a stable and well-defined temperature. The first step in designing this system is to collect the requirements of the various components. These requirements are summarized in Tables 1 and 2. In these tables, the power consumption is the amount of energy used by the component, while the heat dissipation is that portion of the energy which does not go to useful work and is considered as a worst-case scenario. Furthermore, the operating temperature is the range in which the component can actually do its work, whereas the maximum temperature is needed for determining the assembly flow and is the temperature above which the component will sustain damage.

One of the challenges of having a highly-integrated system is that the requirements for the module as a whole are limited by the most restrictive requirements of each component. If the system was less integrated, components that dissipate a fair amount of heat but that have a more flexible operating range, such as the TriPleX chips and phase modulators, could be partitioned from components that have a more limited or demanding operating temperature, such as the tunable lasers. In the end, the sizing of the thermal management system was based on the combined heat dissipation of the transmitter and receiver (16.75 W) and the most restricted operating temperatures of the components (20 °C–25 °C).

The thick copper submount on which these components sit is a design inherited from the LioniX CPS characterization package submount. By introducing a large thermal mass between the thermoelectric cooler (TEC) and optical subassembly, this concept trades some of the responsivity of the TEC for overall temperature

Table 1: Transmitter Thermal Breakdown

Transmitter components	Max. Power Consumption (W)	Max. Heat Dissipation (W)	Operating Temperature (°C)	Maximum Temperature* (°C)
Tunable lasers (InP, 3x)	6.9	3.9	25	100
Phase modulator (InP) (incl. driver)	2.0	2.0	20–50	260
TriPleX (SiN)	2.0	2.0	20–60	150
Antenna chip (InP)	1.0	0.8	25	100
Photonic motherboard (PolyBoard)	0.65	0.65	25	100

* For curing and solder reflow in later assembly steps

Table 2: Receiver Thermal Breakdown

Transmitter components	Max. Power Consumption (W)	Max. Heat Dissipation (W)	Operating Temperature (°C)	Maximum Temperature* (°C)
Tunable lasers (InP, 3x)	6.9	3.9	25	100
Phase modulator (InP)	2.0	2.0	20–50	260
Antenna chip (InP, incl. TIA)	1.0	0.8	25	100
Photonic motherboard (PolyBoard)	0.7	0.7	25	100

* For curing and solder reflow in later assembly steps

stability. A different option would have been to place the TEC directly under the optical assembly, in which case care would need to be taken with the closed-loop parameters of the control circuit so that temperature overshoots would not occur.

Due to the precise control required over the temperature, a Peltier TEC was chosen as the temperature regulator. While this has the advantage of a quick reaction time and compact size, it is not a particularly efficient component and places additional demands on the system heat sinking. The consequence of this is that the sizing of the heat sink is actually almost more important than the sizing of the TEC itself. For the first prototypes, the largest heat sinks with fans that could practically fit in the available area were chosen. These were picked as a pair and connected to the hot side of the TEC via a copper heat bus (Fig. 6). This heat bus turned out to be quite heavy, and in future iterations will be replaced with much lighter copper heat pipes, which act as a sort of thermal superconductor.

The effective thermal resistance of the heat sinking portion of the system was calculated by considering each heat sink and fan individually and then halving the resulting value considering that there are two of each operating in parallel. Because the calculation considers the longest path, it should be taken as a worst-case scenario. A summary of the calculation is shown in Table 3. The final thermal resistance of 0.51 K/W will be used for the TEC calculations.

Now, it is important to understand the caveats of using a Peltier TEC. There is a reason that TECs are not used in refrigerators. They are ideally used in systems where the heat dissipation is low but a large temperature difference is required. If we instead have a large heat load, the hot side of the TEC will increase in proportion with the thermal resistance to the ambient environment. This means that the temperature delta that the TEC needs to generate will increase. Because the TEC is not particularly efficient, this results in more waste heat generated by the TEC itself, which raises the hot side temperature, which raises the required temperature delta, and so on.

When sizing the TEC, it is important to understand the parameters and performance of the TEC. One of the

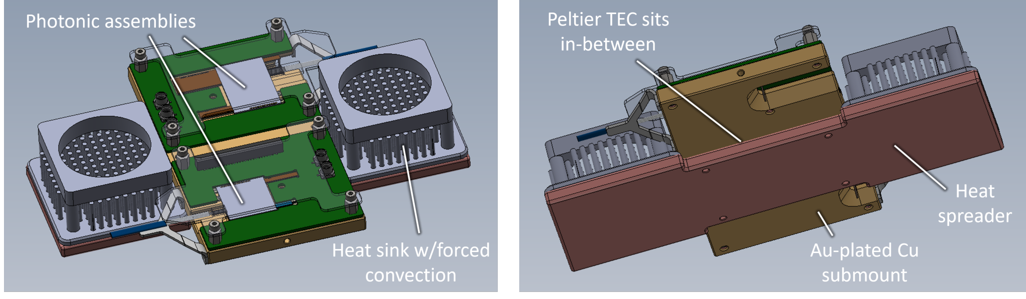

Figure 6: Schematic of thermal subsystem showing forced convection heat sinks and copper heat bus

Table 3: Thermal Resistance Calculation

Heat Bus Width (mm)	40
Heat Bus Thickness (mm)	7
Incremental Thermal Resistance ($\mathrm{K\,W^{-1}\,mm^{-1}}$)	9.3×10^{-3}
Longest Path TEC $\rightarrow$ Heat Sink (mm)	22
Heat Bus Thermal Resistance (K/W)	0.20
Heat Sink Thermal Resistance (K/W)	0.81
Total Thermal Resistance (One Side)	1.01
Total Thermal Resistance (Two Sides in Parallel)	0.51

key parameters is the maximum heat or Q_{max}. Naively, one would assume that this is the heat that a TEC could handle for normal applications, such that a TEC with Q_{max} of 20 W would then be a good candidate for our system with heat dissipation of 16.75 W. However, this interpretation is wrong. The Q_{max} is the heat dissipation at which the TEC does nothing but pass heat through. In other words, it does not provide any temperature difference at this heat flow. A more useful heuristic is to take the desired heat dissipation and multiply it by five and then search for a TEC with that amount of Q_{max}.

Furthermore, when looking at ΔT_{max}, the maximum temperature drop of the TEC, it is not wise to just take the heat dissipation and multiply it by the thermal resistance of the heat sink to find the hot side temperature and then consider the delta between this and the operating temperature. One has to remember that the TEC itself is a relatively inefficient device, and so the amount of heat generated on the hot side is in reality going to be more like 1.5× to 2.0× that of the heat drawn in at the cold side.

For the first prototype, a TEC from RMT Ltd. was selected. This TEC (2x1MC06-142-03) is actually two TECs bonded in parallel and is one of the most powerful compact TECs offered by RMT. While it is tempting to think that way, it should be noted that simply putting two TECs together will not double the capacity of the TEC. To truly realize a doubling of the capability, the thermal resistance of the heat sink would also need to be halved, otherwise the higher temperature at the hot side of the two TECs would drive them into their less efficient operating regimes.

This TEC, when combined with an ideal heat sink, has a Q_{max} of 104.05 W and a ΔT_{max} of 67 K. When combined with the real heat sinking system from the calculations above, these values reduce significantly to 28.16 W and 32 K, respectively. To find the actual operating point for the first TERAWAY prototype, in-house software at PHIX was used. This software can read the datasheets of multiple TEC vendors, interpolate the curves from these datasheets and calculate the various operating points given a fixed thermal resistance. It will also provide specific values given a desired system ΔT, i.e., the difference from the module temperature to the ambient temperature. An example of the output of this software is shown in Fig. 7. This result shows that the copper submount of the optical assembly can be held at around 20 °C in a warm room temperature environment of 300 K (26.85 °C). It also shows that there is quite a bit of margin for over-cooling by up to approximately

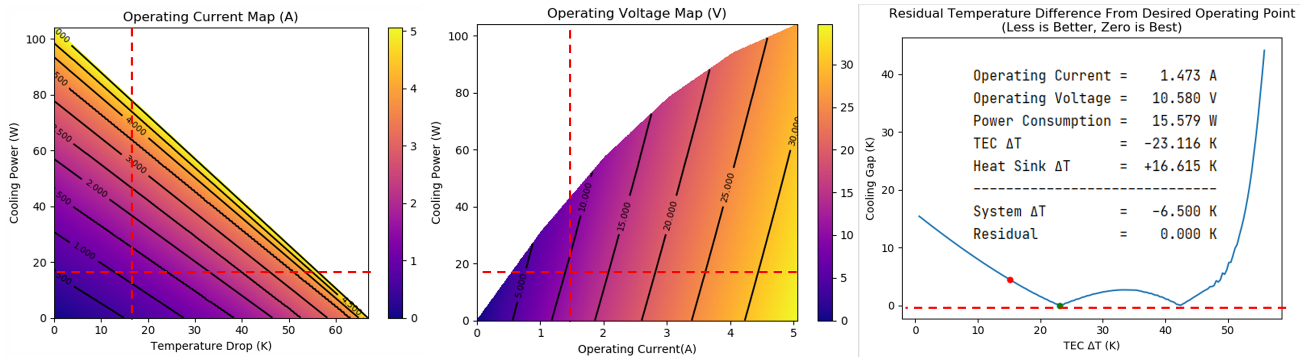

Figure 7: Calculation of Peltier thermoelectric cooler operating points for combined transmitter and receiver

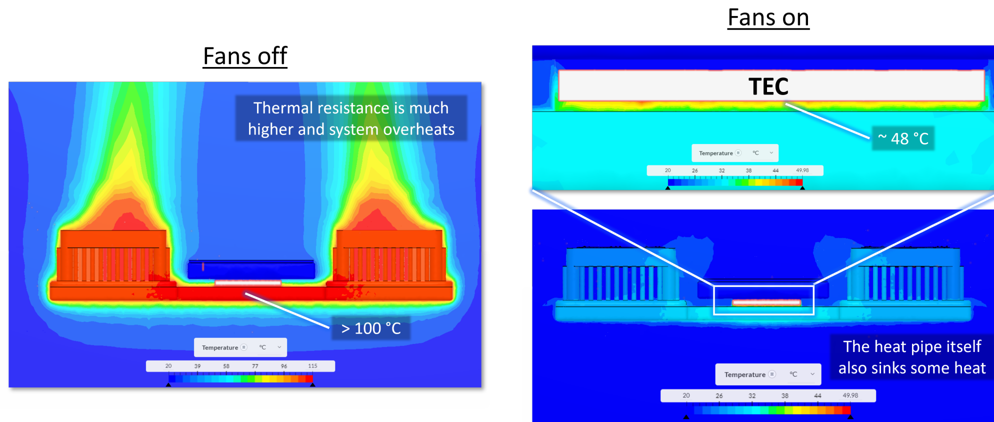

Figure 8: Conjugate heat transfer simulation results of complete prototype module

4 °C. This is the region in the rightmost graph between 23 °C and 42 °C on the horizontal axis.

Finally, the entire design is verified in a conjugate heat transfer simulation using the cloud-based commercial software SIMSCALE. This enables us to check if our previous assumptions were valid and also to see the effect of, for instance, running the system without forced convection on the heat sinks. It should be noted that in this type of simulation, the TEC cannot be efficiently modeled directly. Instead, it is approximated by internal boundary conditions of fixed temperature and heat flow. The results (Fig. 8) indicate that leaving the fans off will result in significant overheating of the system due to the large increase in thermal resistance to the ambient environment. However, when the fans are run, we see the system behaving well. In particular, the hot side of the TEC is approximately 48 °C, which compares well to the expected value of 43.5 °C from the previous calculations.

6. CONCLUSIONS

Optical interfacing, wireless transmission (antenna rod), and thermal management of a highly-integrated mobile 5G transceiver have been discussed in detail in this manuscript. Different strategies of aligning and affixing photonic components from dissimilar fabrication platforms have been presented, with insight into the construction of first prototypes and outlook on scaling. A modified flip-chip process with a molded fixture fabrication process amenable to handling items with complex geometries was shown. Finally, the challenges of maintaining a steady thermal state for closely-linked components with disparate and demanding heat dissipation and operating temperature requirements were laid out, and an example of sizing various thermal system components was given.

This work covered only the first prototype in the TERAWAY project. This prototype had limited functionality, but it was an important first step on the path to realizing a fully-featured mobile 5G transceiver unit. Future work will increase the complexity of the photonic circuits to include beam steering and coherent detection. To

enable this, the antenna rod will go from a single rod to a 1×4 array and finally to a 4×4 array. In parallel, the heat sinking system will be further improved to include lightweight heat pipes, thus decreasing the total payload of the module in the drone.

ACKNOWLEDGMENTS

This work was supported in part by the European Union's Horizon 2020 Research and Innovation Programme through the TERAWAY project (G.A No 871668), which is an initiative of the Photonics Public Private Partnership. Photographs of the completed module and close-up of antenna rod on finished module are courtesy of PHIX and Gijs van Ouwerkerk. The authors would also like to thank Ralph Schachler for support, insight and inspiration with using the Finetech flip-chip systems.

REFERENCES

[1] Giordani, M., Polese, M., Mezzavilla, M., Rangan, S., and Zorzi, M., "Toward 6g networks: Use cases and technologies," *IEEE Communications Magazine* **58**(3), 55–61 (2020).

[2] "TERAWAY | Terahertz technology for ultra-broadband and ultra-wideband operation of backhaul and fronthaul links in systems with SDN management of network and radio resources." https://ict-teraway.eu/ (2021). Accessed: 2021-12-27.

[3] Tsokos, C., Andrianopoulos, E., Raptakis, A., Lyras, N., Gounaridis, L., Groumas, P., Avramopoulos, H., and Kouloumentas, C., "Optical Beamforming Networks Supporting Multibeam and Multicast Operation," *2020 22nd International Conference on Transparent Optical Networks (ICTON)* (2020).

[4] Smith, J., Naftaly, M., Nellen, S., and Globisch, B., "Beam Profile Characterisation of an Optoelectronic Silicon Lens-Integrated PIN-PD Emitter between 100 GHz and 1 THz," *Applied Sciences* **11**(2), 465 (2021).

[5] Nellen, S., Lauck, S., Schwanke, G., Deumer, M., Kohlhaas, R. B., Liebermeister, L., Schell, M., and Globisch, B., "Radiation pattern of planar optoelectronic antennas for broadband continuous-wave terahertz emission," *Optics Express* **29**(6), 8244 (2021).

[6] Ali, M., Garcia-Munoz, L. E., Nellen, S., Globisch, B., and Carpintero, G., "High-speed Terahertz PIN Photodiode with WR-3 Rectangular Waveguide Output," *2020 45th International Conference on Infrared, Millimeter, and Terahertz Waves (IRMMW-THz)* (2020).

[7] Guzmán, R., González, L., Zarzuelo, A., Cuello, J., Ali, M., Visscher, I., Grootjans, R., Epping, J., Roeloffzen, C., and Carpintero, G., "Widely Tunable RF Signal Generation Using an InP/Si_3N_4 Hybrid Integrated Dual-Wavelength Optical Heterodyne Source," *Journal of Lightwave Technology* **39**(24), 7664–7671 (2021).

[8] Tsokos, C., Andrianopoulos, E., Raptakis, A., Lyras, N., Gounaridis, L., Groumas, P., Timens, R., Visscher, I., Grootjans, R., Wefers, L., Geskus, D., Klein, E., Avramopoulos, H., Heideman, R., Kouloumentas, C., and Roeloffzen, C. G. H., "True Time Delay Optical Beamforming Network Based on Hybrid InP-Silicon Nitride Integration," (2021).

[9] Carpintero, G., González, L., Guzmán, R., Ali, M., Felipe, D. D., Qian, T., Keil, N., Grootjans, R., and Roeloffzen, C., "Photonic Integrated Circuits for Terahertz Communication: The Hybrid Integrated Microwave Photonic Approach," *Optical Fiber Communication Conference (OFC) 2021* (2021).

[10] "Standard Package Types - PHIX | Photonics Assembly." https://www.phix.com/our-offering/standard-package-types/ (2021). Accessed: 2021-12-26.